THE
CHEMICAL
RECORD

Surface and Interface Engineering of Graphene Oxide Films by Controllable Photoreduction

Yu-Qing Liu,[a] Yong-Lai Zhang,*[a] Yan Liu,[c] Hao-Bo Jiang,[a] Dong-Dong Han,[a] Bing Han,[a] Jing Feng,[a] and Hong-Bo Sun*[a,b]

ABSTRACT: We report herein the engineering of the surface/interface properties of graphene oxide (GO) films by controllable photoreduction treatment. In our recent works, typical photoreduction processes, including femtosecond laser direct writing (FsLDW), laser holographic lithography, and controllable UV irradiation, have been employed to make conductive reduced graphene oxide (RGO) microcircuits, hierarchical RGO micro-nanostructures with both superhydrophobicity and structural color, as well as moisture-responsive GO/RGO bilayer structures. Compared with other reduction protocols, for instance, chemical reduction and thermal annealing, the photoreduction strategy shows distinct advantages, such as mask-free patterning, chemical-free modification, controllable reduction degree, and environmentally friendly processing. These works indicate that the surface and interface engineering of GO through controllable photoreduction of GO holds great promise for the development of various graphene-based microdevices.

Keywords: graphene, laser chemistry, photochemistry, reduction, surface analysis

1. Introduction

As early as 1859, a compound of carbon, oxygen, and hydrogen was successfully prepared by treating natural graphite with strong oxidizers.[1] The as-obtained material, known as graphite oxide, is a yellow solid of carbon with plenty of oxygen-containing groups (OCGs). A century later, Hummers and Offeman, improved the preparation method, so that graphite oxide could be produced in a much safer and more efficient manner.[2] Graphite oxide was not paid much attention until 2004, when Geim and Novoselov at The University of Manchester successfully obtained a single layer of graphite, named graphene, through a micromechanical cleavage technique with the help of tape.[3] Since graphene reveals a series of outstanding properties, such as ultrahigh carrier mobility,[4] high electrical conductivity,[5] high thermal conductivity,[6] high Young's modulus,[7] high chemical/physical stability,[8] optical transmittance,[9] flexibility,[10] and bio-compatibility,[11] the single-atom-thick carbon crystal rapidly emerged as a rising star on the horizon of materials science. Nowadays, graphene and its related materials have been thoroughly investigated in both fundamental science and practical applications.

In the beginning, single- or few-layer graphene was prepared by mechanical exfoliation, which had very low efficiency. The limitation in graphene preparation significantly restricts

[a]Y.-Q. Liu, Y.-L. Zhang, H.-B. Jiang, D.-D. Han, B. Han, J. Feng, H.-B. Sun
State Key Laboratory on Integrated Optoelectronics
College of Electronic Science and Engineering
Jilin University, 2699 Qianjin Street
Changchun 130012 (P.R. China)
Fax: 86-431-85168281
Tel: 86-431-85168281
E-mail: yonglaizhang@jlu.edu.cn
[b]H.-B. Sun
College of Physics, Jilin University
2699 Qianjin Street, Changchun 130012 (P.R. China)
E-mail: hbsun@jlu.edu.cn
[c]Y. Liu
Key Laboratory of Bionic Engineering (Ministry of Education)
Jilin University, Changchun 130012 (P.R. China)

rapid progress of graphene-based devices. As an alternative choice, graphite oxides have been successfully used as a raw material for the mass production of graphene-like materials in a cost-effective manner.[12] After drastic oxidation of graphite, the π–π conjugation has been broken due to the grafting of various OCGs, such as hydroxyl, epoxy, and carboxyl groups. Thus, the interlayer spacing of graphite oxide becomes much larger and more irregular than that of pristine graphite.[13] As a result, single-layer graphene oxide (GO) could be easily exfoliated in water with the help of ultrasonic treatment. However, the presence of abundant OCGs on a GO sheet makes it isolating, which significantly limits its applications in electronics. Consequently, enormous research efforts have been devoted to the removal of OCGs on GO sheets to restore the conjugated structure and recover their conductivity.[14] Typically, GO could be reduced through either thermal annealing under inert gases[15] or chemical reduction with the help of reducing agents, for instance, hydrazine.[16] After moderate reduction treatment, the majority of OCGs could be effectively eliminated. As a result, the sp^2 region could be partially restored, which rendered certain conductivity to the reduced graphene oxide (RGO). In addition to thermal and chemical reduction protocols, in recent years, photoreduction of GO has emerged as an appealing alternative, since it permits exquisite control over the contents and distribution of OCGs on the GO sheets.[17] Photoreduction of GO starts with the photocatalytic reduction of an aqueous suspension of GO, in which TiO$_2$ has been used as a photocatalyst and the reduction mechanism involves a photochemical process.[18] Later, a high-power xenon lamp was employed to remove OCGs from GO in a photothermal procedure.[19] Compared with conventional thermal/chemical protocols, the photoreduction strategy shows distinct advantages of low cost, high efficiency, and environmental friendliness, so research interests with respect to the photoreduction of GO continue to intensify.[20]

We started research on the femtosecond laser reduction of GO as early as 2008. At the end of 2009, we reported our work entitled "Direct imprinting of microcircuits on GO films by femtosecond laser reduction" in the journal *Nano Today*.[21] At almost the same time, Loh's group also reported the direct laser writing mediated microstructuring of GO using a continuous-wave diode laser.[22] The two works open up a new way for the flexible reduction and patterning of GO through a chemical- and mask-free manner. In addition to the effective reduction of GO, laser treatment synchronously exhibits additional advantages, for instance, designable patterning, micronanostructuring, and the formation of highly porous structures with high surface areas. Nowadays, the photoreduction methodology has been widely recognized as a powerful tool for engineering the surface and interface properties of GO films. Herein, we briefly summarize our recent progress in the controllable photoreduction of GO for diverse applications.

2. Fundamentals of Photoreduction of GO

Despite the fact that graphite oxide has been successfully prepared for many years, the precise chemical structure of GO is

Yu-Qin Liu received her B.S. from the College of Electronic Science and Engineering (2015), Jilin University. She is currently a Ph.D. student in the State Key Laboratory of Integrated Optoelectronics, Jilin University. Her research work focused on graphene and graphene-related materials. Her current research interests include laser modification of graphene oxides, biomimetic graphene surfaces, and graphene-based functional devices.

Yong-Lai Zhang received his B.S. (2004) and Ph.D. (2009) degrees from Jilin University, P.R. China. Then, he joined the faculty of the State Key Laboratory on Integrated Optoelectronics, College of Electronic Science and Engineering, Jilin University. In 2011, he worked as a Research Professor in Yonsei University, Korea. After that, he was awarded a "Hong Kong Scholar" postdoctoral fellowship and worked at the Center of Super Diamond and Advanced Films (COSDAF), City University of Hong Kong. His research interests include laser micro-nanofabrication of functional micro-nanostructures, smart actuators, and Bio-MEMS.

Hong-Bo Sun received his Ph.D. from Jilin University, P.R. China, in 1996. He worked as a Postdoctoral Researcher at the University of Tokushima, Japan, from 1996 to 2000, and then as an Assistant Professor in the Department of Applied Physics, Osaka University. He became a project leader in 2001. He received an award from the Optical Science and Technology Society in 2002, and won an Outstanding Young Scientist Award issued by the ministry of MEXT (Japan) in 2006. In 2005, he became a Professor (Changjiang Scholar) at Jilin University. His research focuses on laser micro-nanofabrication and their applications in micro-optics, micromachines, microfluids, and microsensors.
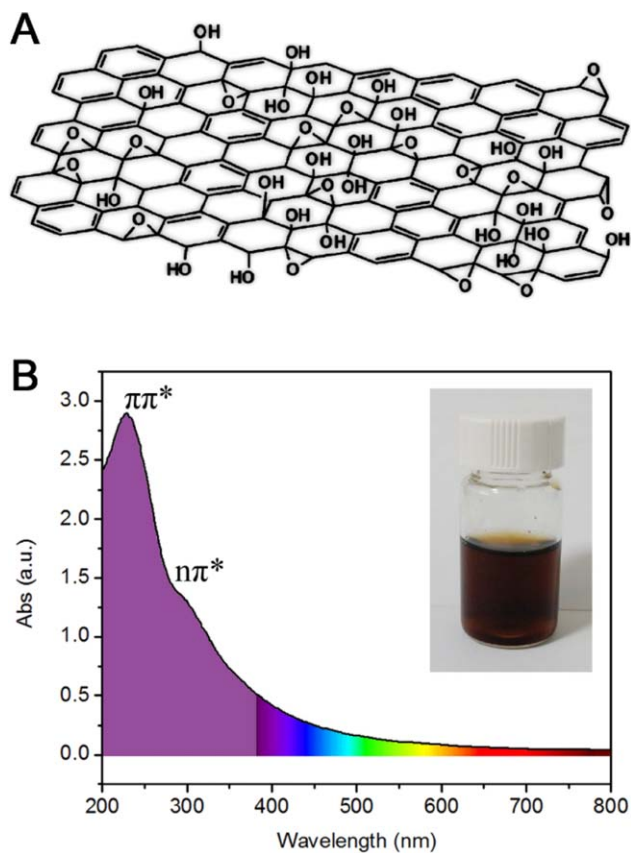
Fig. 1. A) Lerf–Klinowski model of GO with randomly distributed OCGs (e.g., carboxyl, carbonyl, ester) on the carbon plane of the graphitic platelets. B) The absorption spectrum of a typical aqueous solution of GO. Inset: a photograph of a bottle containing an aqueous solution of GO.

still uncertain. The concentration and distribution of OCGs on a GO sheet may be different, so it is impossible to find the same GO sheets in an aqueous solution of GO. Currently, GO is prepared mostly based on a modified Hummers method. However, GO prepared from different raw graphite or with different degrees of oxidation may be totally different in both chemical structure and composition. Generally, a nonstoichiometric GO model proposed by Lerf and Klinowski is widely accepted.[23] As shown in Figure 1A, the sp²-carbon plane is randomly decorated with various OCGs, such as hydroxyl, epoxy, and carbonyl groups. Generally, the aqueous suspension of GO is yellow–brown in color (Figure 1B). The UV/Vis absorption spectrum of GO shows that GO has a strong absorption below 400 nm, with a characteristic shoulder at 305 nm attributed to n–π* transitions of C=O bonds.[24] According to this spectrum, UV irradiation seems to be a preferred light source for GO reduction. However, since GO also demonstrates certain adsorptions throughout the visible-light range from 380 to 780 nm, various irradiations ranging from a 400 nm Xe lamp to a femtosecond laser at about 800 nm have

also been successfully adopted for GO reduction.[21,25] The effective conversion of photoenergy into either thermal or chemical energies that could induce the removal of OCGs on GO sheets is the essence of GO reduction.

Smirnov et al. investigated the threshold for the photochemical reduction of GO, in which the required photon energies should be larger than 3.2 eV.[26] In other words, irradiations with a wavelength smaller than 390 nm can trigger the deoxygenation reaction in a photochemical way. Otherwise, the photoreduction mechanism could be attributed to a photothermal effect, excluding cases of multiphoton absorption. Generally, after photoreduction, the color of GO changes from yellow–brown to black, the characteristic shoulder of GO at 305 nm disappears, and the absorption band of GO at 230 nm redshifts to about 270 nm due to π–π* transitions of extended aromatic C-–C bonds, which indicates that electronic conjugation within the graphene sheets is partially restored. However, it is necessary to note that it is not appropriate to refer to RGO as graphene, since the residual OCGs and defects alter the properties dramatically. Nevertheless, despite the fact that it is impossible to fully restore the graphene structure through a reduction treatment of GO, the photoreduction methodology still reveals great potential for tailoring the structure and composition of GO in a controlled manner.

3. Femtosecond Laser Direct Writing (FsLDW) for Designable Patterning

3.1. Photoreduction and Patterning of GO

Femtosecond laser direct writing (FsLDW) has been widely recognized as a powerful tool for making micro-nanostructures with high resolution, arbitrary shape, and even 3D configurations.[27] Generally, it is performed by scanning a tightly focused laser beam, according to a pre-designed patterns; the processes are usually based on photopolymers. FsLDW was successfully used for the reduction and synchronous patterning of GO as early as 2009.[21] At that time, the photochemical reduction of GO with the help of TiO₂ photocatalysts and photothermal reduction of GO using a camera flash were successfully reported;[19] the laser reduction of GO is still rare. According to the absorption spectrum of GO (Figure 1B), a UV laser seems to be a good choice for GO reduction. For femtosecond laser pulses, the wavelength is about 800 nm, at which GO shows very low absorption. Therefore, it is somewhat enigmatic to use a femtosecond laser to reduce GO. However, we successfully observed a clear color change of GO from yellow–brown to black upon the irradiation of a focused femtosecond laser beam, and confirmed the effective reduction of GO by further characterization. Notably, the duration of a femtosecond laser pulse is only 120 fs, so the instantaneous
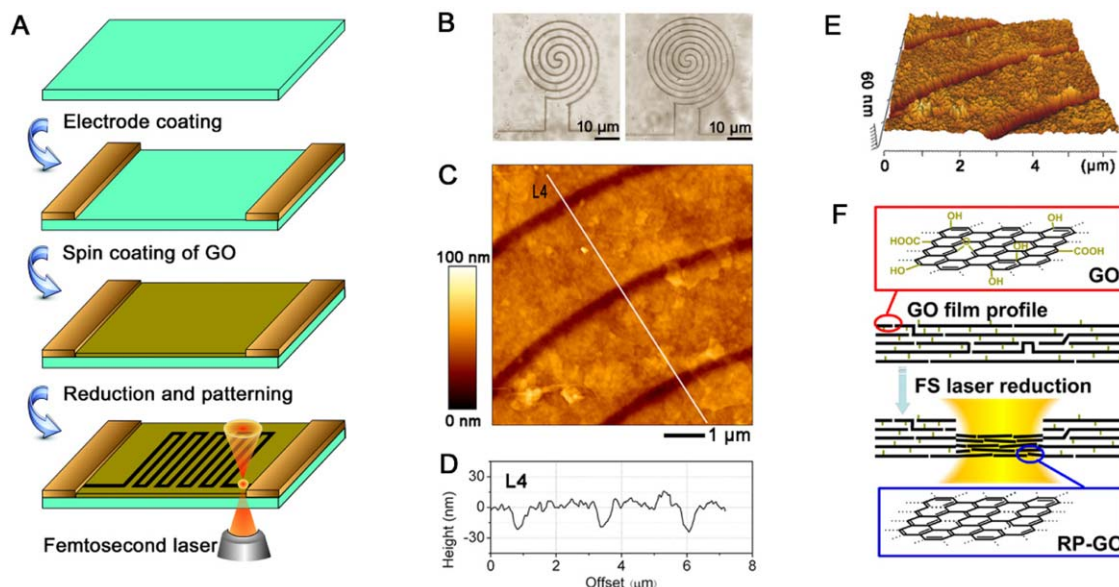
Fig. 2. A) Preparative scheme of using FsLDW to prepare RGO micropatterns. B) Optical microscopy images of RGO patterns. C) AFM image of the patterned RGO film. D) Height profile along the white line in C). E) 3D image of C). F) Schematic illustration of the profile of the GO film before and after FsLDW.

intensity of a laser pulse can reach a very high value. Since thermal relaxation could be suppressed in the case of femtosecond laser processing, multiphoton absorption would account for the reason why a femtosecond laser is workable for GO reduction.

Figure 2A shows the procedure of making conductive RGO micropatterns on a GO film by FsLDW. Typically, an aqueous suspension of GO was spin coated on a glass substrate to form a continuous GO film. Then the GO film was reduced by scanning a focused femtosecond laser according to preprogrammed patterns. The as-formed micropatterns could be clearly identified from optical microscopy images due to poor transparence in the RGO region (Figure 2B). We further examined the surface topography of the micropatterns by AFM. As shown in Figure 2C–E, micropatterns with sunken surfaces could be clearly observed. The height profile along the white line in Figure 2C shows that the line is 500 nm wide, which indicates the high resolution of the RGO micropatterns. Figure 2F illustrates the profile of the GO film before and after FsLDW. The formation of a sunken surface at the laser-scanned region could be attributed to the removal of OCGs in the form of various carbon species (e.g., CO, CO_2). The surface topography of RGO patterns fabricated by FsLDW was different from other laser-induced GO reductions reported,[20a,20b,28] in which laser irradiation led to clear expansion. FsLDW-induced reduction of GO was further confirmed by X-ray photoelectron spectroscopy (XPS). Notably, the content of carbon not bound to oxygen in pristine GO is estimated to be about 44%, whereas RGO shows much higher content of about 61% after FsLDW; this indicates the effective

removal of OCGs. However, despite OCGs being effectively removed, the sp^2 region is not fully restored. Raman spectra show that the D/G intensity ratio (I_D/I_G) even slightly increased from 0.83 with respect to pristine GO to 0.89 after FsLDW reduction, since the drastic laser treatment would break relatively large GO sheets into small pieces, which generates more defects.[29] Nevertheless, the RGO patterns become conductive after FsLDW reduction, which makes it possible to directly "write" microcircuits on a GO film. Moreover, the resistivity of the resultant RGO could be tuned by using different laser intensities. Figure 3A shows the dependence of resistivity and conductivity of the as-obtained RGO microbelts on different output powers of the femtosecond laser. Clearly, with increasing laser power, the conductivity increased and the resistivity decreased accordingly. The highest conductivity of 2.56×10^4 S m^{-1}, together with the lowest resistivity of 3.91×10^{-5} Ωm, have been achieved under the highest laser power of 3.0 mW, above which the thin GO film would be totally ablated. The resistance of the RGO micropatterns further depends on the width and film thickness. As shown in Figure 3B, the comb-like and dual-curvilinear microcircuits give different resistances of 2.1 and 7.8 MΩ, respectively.

In addition to the reduction and patterning of GO, the femtosecond laser treatment also permits refined control over the contents and distributions of OCGs.[30] By tuning the laser power within a certain range, the contents of residual OCGs could be modulated from about 50% oxygen with respect to some highly oxidized GO to <10% after thorough laser reduction. It is known that graphene is a zero band-gap semiconductor; its applications in electronics has been significantly

restricted due to the absence of a band gap. Currently, tailoring the band gap of graphene is still a big challenge. From a practical point of view, heteroatom doping has been recognized as an effective way to open up the band gap. Providing oxygen could be considered as a dopant, the electronic band structures of RGO could be modulated accordingly through controllable laser treatment. As a typical work, we successfully prepared metallic RGO under high-power laser reduction, whereas

semiconductor RGO was achieved under moderate laser intensity.

3.2. Nitrogen Doping and Patterning

Apart from the modulation of the oxygen content, simultaneous nitrogen doping could be achieved when the laser treatment was implemented in an NH_3 atmosphere.[31] To realize FsLDW processing in ammonia, the GO film on a glass substrate was tightly covered by a polydimethylsiloxane (PDMS) cavity with an inlet connected to the NH_3 source and an outlet connected to an acid recycling pool. In this way, the reduction and nitrogen doping of GO was achieved synchronously by scanning a tightly focused femtosecond laser on the GO film, according to preprogrammed micropatterns. Notably, reduction and doping can only occur in the area irradiated by laser focus, N-doped RGO could be directly shaped into various micropatterns of high resolution. The presence of N species in the resultant RGO was confirmed by XPS. As shown in Figure 4, the C 1s spectra were deconvoluted into four Gaussian peaks that corresponded to C−C (284.6 eV), C−N (285.8 eV), C−O (286.6 eV), and C=O (288.5 eV), respectively. Compared with pristine GO, which only shows C and O signals, the laser-treated samples show clear N signals accompanied by a decrease in the oxygen signals, which indicates the reduction and N doping of GO.

Figure 4B shows the N 1s XPS spectra with peaks at 398.2, 399.7, and 401.7 eV, corresponding to pyridinic-, pyrrolic-, and graphitic-N, respectively. According to the formation energy of different N species calculated from a first-principles study, the formation of graphitic-N seems to be much easier, since its formation energy is much lower than those of pyridinic- and pyrrolic-N. However, more than half of
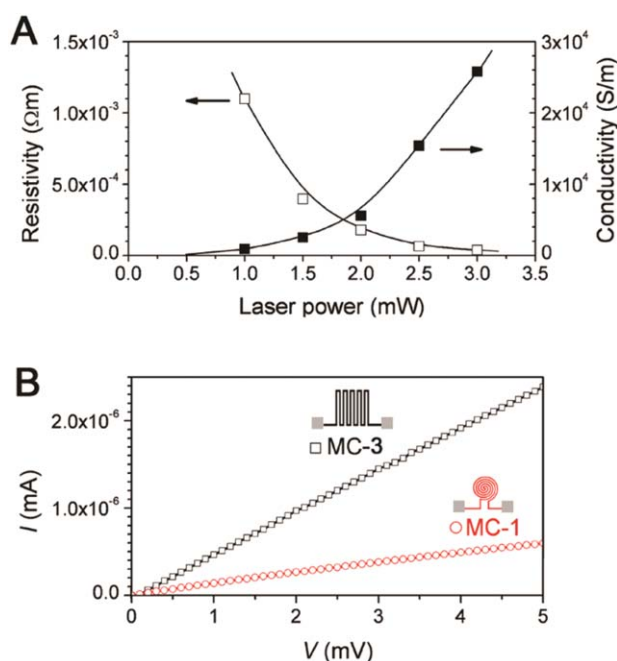
Fig. 3. A) Dependence of resistivity and conductivity of RGO prepared by FsLDW on relative laser power. B) Current–voltage curves of different RGO microcircuits.
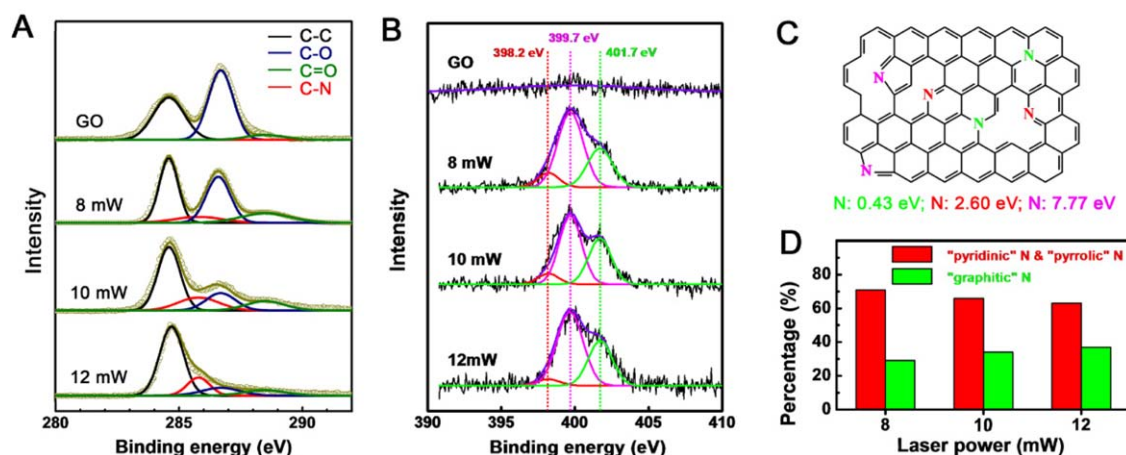
Fig. 4. A) C 1s XPS spectra of GO and N-doped RGO prepared under different laser powers. B) N 1s spectra of GO and N-doped RGO prepared under different laser powers. C) Schematic illustration of the N-doped RGO and the corresponding formation energy calculated from a first-principles study. D) The percentage of pyridinic-/pyrrolic- and graphitic-N of N-doped RGO prepared under different laser powers.

the N atoms are doped in the form of pyrrolic-N because OCGs and defects on GO sheets facilitate the formation of pyrrolic-N. Nevertheless, with increasing laser power, more N atoms are substitutionally doped into the graphene lattice in the form of graphitic-N. Since graphitic-N contributes mainly to the n-type behavior, processing at a higher laser power would be effective at achieving n-type graphene. Herein, the highest N concentration is 10.3% and the percentage of graphitic-N is about 30%. Compared with a conventional doping method, such as electrical annealing,[32] thermal/hydrothermal treatment,[33] in situ chemical vapor deposition (CVD) growth in the presence of ammonia,[34] N$^+$-ion irradiation,[35] and microwave plasma treatment,[36] FsLDW-induced N doping shows unique advantages of a high doping concentration, mask-free patterning, and good compatibility with device integration.

3.3. Device Fabrication

In fact, photoreduction strategies not only permit exquisite control over the oxygen and nitrogen contents, but also provide compatible processing flow with state-of-the-art technologies used for device fabrication. In our previous work, the RGO channel could be post-integrated with a field-effect transistor (FET) device,[30] in which the source/drain electrodes, gate, and gate dielectric layer were prepared beforehand. More importantly, FsLDW permits conductive RGO micropatterns to be made with arbitrary shapes; this provides an opportunity to design and fabricate RGO electrodes for microdisplay devices, such as microscale organic light-emitting devices (micro-OLEDs). As a typical example, we have demonstrated the fabrication of arbitrarily shape customized micro-OLEDs by employing RGO micropatterns prepared by FsLDW as the anode of the devices.[37] Figure 5A shows a schematic illustration of the patterning of RGO electrodes. A RGO micropattern was directly written on the GO film by scanning a focused laser beam according to a preprogrammed pattern. Then, the micro-OLEDs based on the patterned RGO anodes were fabricated with the structure RGO/m-MTDATA (30 nm)/NPB (20 nm)/Alq$_3$ (50 nm)/LiF (1 nm)/Al (100 nm), as shown in Figure 5B. Interestingly, complex patterns, for instance, bowknot-shaped micro-OLEDs, could be readily prepared using this method. As shown in Figure 5C–F, the bowknot-shaped micro-OLEDs show well-defined shapes and edges, as well as uniform electroluminescence emission. With the help of FsLDW, micro-OLEDs with any desired patterns could be readily fabricated based on patterned RGO electrodes. These works may open the door for new applications in microdisplays and three-dimensional or flexible displays.
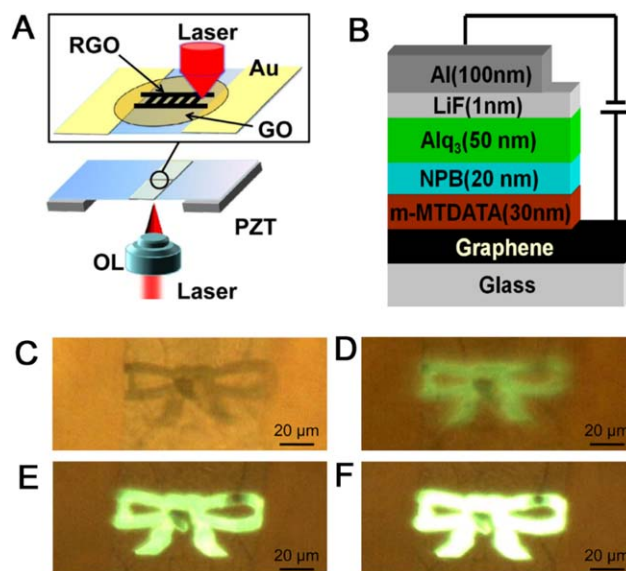

Fig. 5. A) Illustration of the preparative procedure for FsLDW-induced reduction and patterning of GO films. B) Schematic structure of an OLED using patterned RGO as the electrode. Alq$_3$=tris(8-hydroxyquinolinato)aluminum, NPB=N,N'-bis(naphthalen-1-yl)-N,N'-bis(phenyl)benzidine, m-MTDATA=4,4',4''-tris [phenyl(m-tolyl)amino]triphenylamine. Bowknot-shaped micro-OLED devices under driving voltages of 0 (C), 5 (D), 7 (E), and 9 V (F).

4. Laser Holographic Lithography for Micro-nanostructuring

In addition to the reduction of GO, laser irradiation would also induce the formation of micro-nanostructures on the resultant RGO films, if the photoreduction treatment has been precisely controlled. As typical examples, Cote et al, reported the flash reduction of GO; the resultant RGO sample shows expanded structures due to the removal of OCGs.[19] Later, Mukherjee et al, found that RGO samples prepared through a photothermal treatment exhibited a unique "open-pore" structure and could be used as anode materials for Li-ion batteries (LIB) or other energy-storage devices.[28a] Apart from a camera flash, the 788 nm infrared laser from a standard LightScribe DVD optical drive has also been used for GO reduction, patterning, and structuring. Kaner's group first reported the laser scribing of RGO electrochemical capacitors and flexible electronics using this method.[20a] Interestingly, the stacked GO sheets could be transformed into highly porous structures that exhibited a surface area as high as 1520 m^2 g-1 after laser scribing treatment. The formation of such a porous structure could be attributed to drastic expansion during the removal of carbon species (e.g., CO, CO$_2$).

In fact, the surface structure of RGO could be precisely tuned by tailoring the light field of lasers. To gain better control over the micro-nanostructures of a photoreduced RGO film, we first reported the two-beam laser interference (TBLI)
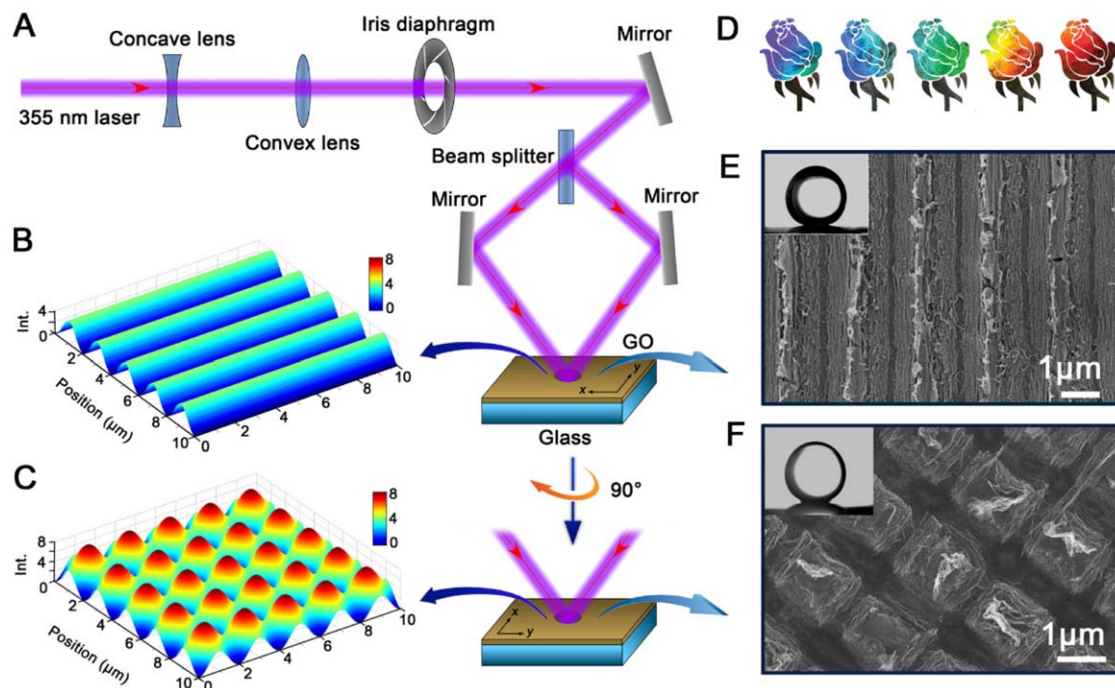
Fig. 6. A) Schematic illustration of the TBLI processing system. The laser intensity distributions of TBLI (B) and dual TBLI treatment with 90° rotation (C) calculated by Matlab. D) Structural color of the structured RGO films. E) SEM image of TBLI-treated GO films with a period of 2 μm. F) SEM image of twice-TBLI-treated GO films with a period of 2 μm. Insets of E) and F) are photographs of a water droplet on the surface; the contact angles (CAs) are 153 and 155°, respectively.

mediated reduction and structuring of GO films.[38] Figure 6A shows a schematic illustration of the TBLI system used for GO reduction and structuring. A frequency-tripled, Q-switched, single-mode Nd:YAG laser (Spectra-Physics) with an emission wavelength of 355 nm, frequency of 10 Hz, and pulse duration of 10 ns has been used as the light source for the experiments. When two laser beams were guided to irradiate at same position of a GO film, interference occurred. In this case, the laser intensity distribution is constant along the y axis and sinusoidal along the x axis. The highest laser intensity could reach four times that of each laser beam, and the minimum value was zero (Figure 6B). When the GO film was exposed to the interferential laser beams, it could be reduced with a similar distribution of exposure intensities; OCGs could be drastically removed in the region of high laser intensity and survived in the low-intensity region. However, this is a theoretic model. In practical experiments, we found that most of the OCGs could be removed due to thermal relaxation, especially when the period was small. In fact, the interference period could be precisely controlled by changing the angle of two laser beams and the as-formed micropatterns of the light-intensity distribution could also been tuned by either multibeam interference or multiple exposure of two-beam interference (Figure 6C). In this regard, the obtained surface structures of the resultant

RGO film could be rationally designed and fabricated using this method.

As a typical example, we prepared biomimetic RGO surfaces that possessed both superhydrophobicity and brilliant iridescence (Figure 6D) by TBLI treatment of GO.[39] This work was inspired by rose petals and butterfly wings, which exhibit similar surface properties. It is well known that the surface structures and chemical composition govern the surface dewetting properties of a solid surface. A general approach to a superhydrophobic surface is to combine hierarchical micro-nanostructures with functional materials that have a low-surface energy.[40] In our work, TBLI-mediated photoreduction of GO provided opportunities for controlling both the surface structures and surface energy synchronously. By tuning the laser power within a certain range, the content of oxygen atoms could be modulated from about 46% with respect to pristine GO to about 6% with respect to RGO. The drastic removal of hydrophilic OCGs in the form of carbon species (e.g., CO_2, CO) and H_2O not only alters the surface energy of the resultant RGO significantly, but also leads to a clear expansion of the stacked GO sheets along the cut edge. In this way, hierarchical structures, including microscale gratings and nanoscale, layered structures, formed without the use of any templates, shadow masks, or chemical reagents. Figure 6E

shows the SEM images of the hierarchically structured RGO surface prepared by TBLI reduction of GO. The RGO surface with microscale gratings with a 2 μm period shows the best hydrophobic properties and a water droplet CA of 153° is achieved. The superhydrophobicity could be attributed to the formation of hierarchical structures and the removal of hydrophilic OCGs.

Notably, the superhydrophobicity of the RGO films with 1D grating structures shows clear anisotropy. Static water CA measurements were recorded both along the grating direction and from the vertical direction, and the CAs in the parallel direction were smaller than those in the perpendicular direction. The anisotropic superhydrophobicity could be overcome by applying another TBLI treatment after rotating the substrate by 90° along the surface normal.[41] As shown in Figure 6E, 2D micropillar arrays with square lattice structures have been successfully fabricated. Interestingly, our superhydrophobic RGO films exhibit unique optical characteristics due to the scattering and diffraction of the grating structures. A uniform transmission diffraction spot could be clearly observed on the received screen when excitation light irradiated the graphene films. Brilliant structural color could be clearly observed by the naked eye (Figure 6D). These results not only provide new insights into the design of colorful superhydrophobic surfaces, but are also beneficial for our understanding of interactions at the liquid–graphene interface.

5. Controllable Photoreduction for Smart Actuation

Smart actuators are devices that can convert various types of energy or environmental signals into mechanical deformation by changing their dimensions. As a typical example, multi- or bilayered structures have been widely used for actuating, since clear deformation could be achieved by simply changing the environmental signals, such as pH,[42] temperature,[43] chemicals,[44] and light.[45] However, general multi-/bilayer actuators are based on metals, polymers, and semiconductors. Concerns with respect to toughness, elasticity, chemical/physical stabilities, and interlayer adhesion constitute a main barrier for the development of robust actuators. Recently, carbon-based 2D materials, graphene and its derivatives, exhibit distinct advantages, such as flexibility,[10] transparency,[9] mechanical strength,[7] high electrical/thermal conductivity,[5,6] biocompatibility,[11] and excellent stability;[8] these hold great promise for the development of robust actuators. As natural 2D materials, solution-processable graphene and related materials (e.g., GO, RGO) are very tractable for the formation of multi-/bilayer structures. In particular, the presence of many OCGs on the GO sheets makes it possible to alter their properties through covalent grafting of various functional groups. However, to achieve stimuli-responsive properties, an asymmetric structure along the lateral section of the GO film is generally necessary. Considering the penetrability and reactivity of the stacked GO sheets, enormous difficulties arise in the selective modification of GO through general chemical or thermal treatments.

From a practical point of view, photoreduction strategies enable controllable modulation of the surface/interface properties of GO films through a mask-free, chemical-free, and cost-effective manner. Previous results reported by us and others have already proved that the photoreduction treatment of GO could significantly change the surface properties by removing the OCGs; this provides the feasibility for the rational design and fabrication of graphene-based smart actuators. For instance, Qu et al. reported the preparation of moisture-responsive graphene fibers by region-selective reduction of the GO fibers using FsLDW.[46] Taking advantage of the "direct writing" feature, the RGO region could be patterned at any desired positions; in this way, well-controlled motion and more sophisticated deformation can be achieved in a predetermined manner once exposed to moisture.

In fact, the region-selective photoreduction of GO is not limited to the use of femtosecond laser pulses. Any light sources that enable the effective removal of OCGs through either photochemical or -thermal processes could be used for the manufacture of graphene actuators. Recently, by using sunlight as an irradiation source, we successfully developed a self-controlled photoreduction method to prepare GO/RGO bilayer films for actuator manufacture.[47] Generally, as soon as the focused sunlight irradiates the GO paper, a clear color change can be observed, which indicates the removal of OCGs on the GO sheets. However, the as-formed RGO layers, which have a clearly expanded structure, would prevent light transmission and suppress the thermal relaxation effectively. As a result, the photoreduction gradient along the lateral direction of thick GO paper could be self-controlled upon light irradiation under moderate intensity. Using this self-controlled photoreduction strategy, a unique GO/RGO bilayer structure with a gradually changing reduction gradient along the lateral section could be obtained without the use of any masks or chemical reagents. Owing to the asymmetric distribution of OCGs, the GO and RGO layers show very different properties in water adsorption under moisture. According to our quantificational calculations based on a first-principles study, GO sheets bearing many OCGs can adsorb water molecules due to the formation of hydrogen bonds, whereas pristine graphene interacts with water molecules through much weaker van der Waals forces. In this regard, when a GO/RGO paper was placed in moisture, more water molecules would be adsorbed by GO layers. Since the adsorption of water would cause a significant expansion in the GO layer, the asymmetric deformation directly leads to reversible bending and straightening performance of the GO/RGO bilayer paper in moist and dry
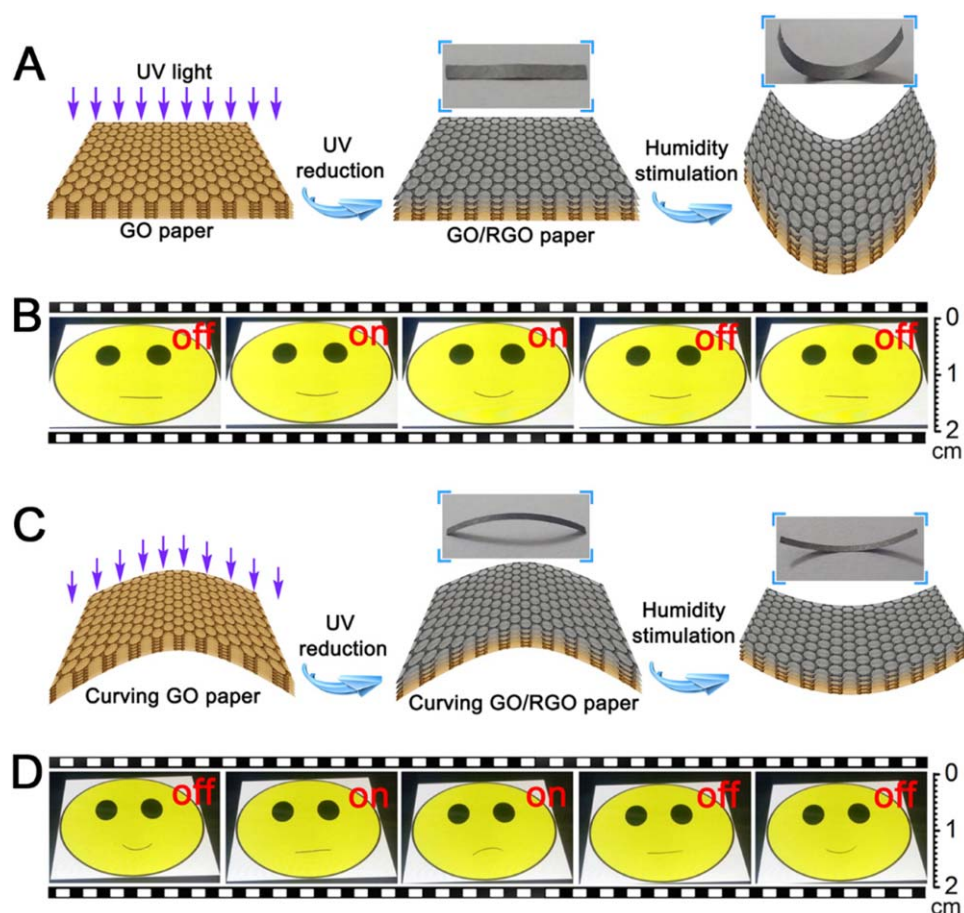
Fig. 7. Schematic illustration of the design principle of GO/RGO bilayer actuators and their predictable responsive properties to environmental humidity. A) Self-controlled photoreduction of flat GO paper. B) Moisture-responsive "smart face" based on flat GO/RGO paper. C) Self-controlled photoreduction of curved GO paper. D) Moisture-responsive "smart face" based on curved GO/RGO paper. The insets are digital photographs of GO/RGO bilayer ribbons in dry and moist conditions.

conditions, respectively. Based on this principle, we designed and fabricated a series of moisture-responsive actuators, including a claw, an orientable object transporter, and a crawler paper robot.

It is well known that GO solution shows strong absorption in the UV region; thus UV light plays a very important role in the controllable photoreduction of GO. Despite the fact that focused lasers or sunlight are capable of making GO/RGO bilayer structures through a self-controlled photoreduction treatment, the pinpoint processing manner with respect to both direct laser writing and focused sunlight irradiation not only limits the fabrication efficiency, but also makes the GO/RGO bilayer not uniform, leading to an unstable response under external stimulus. To make uniform and large GO/RGO bilayer structured papers, we subsequently developed a unilateral UV irradiation method (Figure 7A and B).[48] Upon UV irradiation, a self-controlled photoreduction could also be

achieved by tuning the irradiation intensity and times. In addition, the initial curvature of the GO paper could be flexibly determined using curved substrates; in this way, the bending degree of the obtained GO/RGO bilayer paper could be tuned freely over a much wider range (Figure 7C, D). Moreover, UV irradiation induced photoreduction permits flexible patterning of RGO using predesigned shadow masks. Through rational design, more complex actions than simple bending could be easily achieved based on the patterned GO/RGO bilayer papers; this provides the feasibility to get better control over their responsive properties. As typical examples, smart humidity-driven graphene actuators that mimicked the cilia of the respiratory tract and a tendril climber plant have been developed for controllable object transport. Self-controlled photoreduction shows unique advantages for the engineering of the surface/interface properties of GO films, and holds great promise for the rational design and fabrication of various smart graphene actuators.

6. Summary and Outlook

We have successfully developed a controllable photoreduction methodology for engineering the surface and interface properties of GO films. For the first time, we found that a focused femtosecond laser beam enabled effective removal of OCGs on GO sheets, and thus, developed a FsLDW-mediated photoreduction method for making conductive RGO microcircuits through a mask-free, chemical-free, and environmentally friendly manner. Furthermore, the FsLDW-induced photoreduction of GO not only allows post-integration processing, but also permits sophisticated control over the residual oxygen content and even doped heteroatoms under special processing conditions, which makes the programmable photoreduction strategy very promising for the flexible design and fabrication of graphene-based electronics.

In addition to controllable reduction, doping, and designable patterning, laser processing also reveals great potential in the structuring of RGO films. As typical examples, laser holographic lithography has been employed for tailoring the surface structures and tuning the surface chemical composition synchronously. The combined effects of hierarchically structuring and removing hydrophilic OCGs endow the resultant RGO film with both superhydrophobicity and brilliant structure color. Moreover, the formation of hierarchical structures represented by microscale gratings and nanoscale, layered structures significantly increased the exposed surface areas of the RGO films, which made them promising candidates towards a wide range of applications, for instance, in sensors and energy-storage devices.

As a controllable reduction strategy, photoreduction of GO provides opportunities to engineer their interface properties through a self-controlled process. It is well known that photon energy gained for GO reduction is derived from the incident light. Therefore, for a typical photoreduction process, the reduction gradient along the lateral section of a GO film is dominated by the light penetration depth and thermal relaxation extent. This self-controlled photoreduction effect inspired us to design and fabricate various stimuli-responsive smart actuators based on the resultant GO/RGO bilayer papers. Interestingly, taking advantage of the unique photoreduction strategy, the responsive properties could be tuned by controlling the degree of reduction; this more complicated performance beyond simple bending could be realized by making desired micropatterns.

Despite promising recent progress, there is still a huge scope to further tailor the surface and interface properties of GO through controllable photoreduction. It is widely recognized that FsLDW is a powerful 3D processing tool. Since 1991, two-photon photopolymerization has been employed to fabricate 3D micro-nanostructures due to the nonlinear absorption effect. To date, the spatial resolution has been
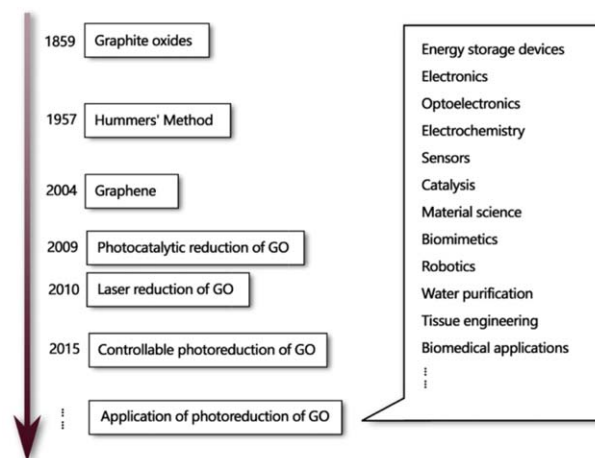

Fig. 8. Schematic illustration of the research background and trends of photoreduction of GO, as well as potential applications of this technology.

improved to tens of nanometers. However, 3D prototyping of graphene-based micro-nanostructures has not been reported yet. The lack of 3D GO or RGO structures could be attributed to the 2D nature of graphene derivatives. Providing a GO microrobot could be 3D-printed directly, further laser 3D modification would make it smart; in this way, the powerful FsLDW tool may realize its full potential.

We summarize the research background and trends of photoreduction of GO in Figure 8. Since the report of the photocatalytic reduction of GO in 2009, the photoreduction strategy has become a preferred approach to produce graphene-like materials from raw GO towards a wide range of applications.[50] However, we have to say it is a pity that GO could not be fully reduced to pristine graphene, just like those prepared from mechanical exfoliation through various reduction protocols, including photoreduction. The residual functional groups and defects dramatically alter the structure of the carbon plane, making the resultant RGO a different material to graphene. However, in turn, the presence of OCGs or defects provides us with additional opportunities to tune their surface and interface properties through various chemical or physical modifications. From this point of view, controllable photoreduction reveals a series of unique advantages, such as mask-free and designable patterning, chemical-free modification, controllable reduction degree, and cost-effective processing, which make the photoreduction protocol very promising for the development of various graphene-based microdevices. Nowadays, with the rapid progress of 2D materials, graphene and graphene derivatives have been widely used in both in fundamental science and practical applications. In this regard, controllable phototreatment is expected to become more and more popular in engineering their surface and interface properties. Perhaps it could be extended to other 2D materials systems[49] in the near future.

Acknowledgements

REFERENCES

[1] B. C. Brodie, *Philos. Trans. R. Soc. London* **1859**, 249–259.

[2] W. S. Hummers, Jr., R. E. Offeman, *J. Am. Chem. Soc.* **1958**, *80*, 1339–1339.

[3] K. S. Novoselov, A. K. Geim, S. Morozov, D. Jiang, Y. Zhang, S. A. Dubonos, I. Grigorieva, A. Firsov, *Science* **2004**, *306*, 666–669.

[4] a) E. Hwang, S. Adam, S. D. Sarma, *Phys. Rev. Lett.* **2007**, *98*, 186806; b) S. Morozov, K. Novoselov, M. Katsnelson, F. Schedin, D. Elias, J. Jaszczak, A. Geim, *Phys. Rev. Lett.* **2008**, *100*, 016602.

[5] Z.-S. Wu, W. Ren, L. Gao, J. Zhao, Z. Chen, B. Liu, D. Tang, B. Yu, C. Jiang, H.-M. Cheng, *ACS Nano* **2009**, *3*, 411–417.

[6] A. A. Balandin, S. Ghosh, W. Bao, I. Calizo, D. Teweldebrhan, F. Miao, C. N. Lau, *Nano Lett.* **2008**, *8*, 902–907.

[7] C. Lee, X. Wei, J. W. Kysar, J. Hone, *Science* **2008**, *321*, 385–388.

[8] Ç. Ö. Girit, J. C. Meyer, R. Erni, M. D. Rossell, C. Kisielowski, L. Yang, C.-H. Park, M. Crommie, M. L. Cohen, S. G. Louie, *Science* **2009**, *323*, 1705–1708.

[9] X. Li, Y. Zhu, W. Cai, M. Borysiak, B. Han, D. Chen, R. D. Piner, L. Colombo, R. S. Ruoff, *Nano Lett.* **2009**, *9*, 4359–4363.

[10] K. S. Kim, Y. Zhao, H. Jang, S. Y. Lee, J. M. Kim, K. S. Kim, J.-H. Ahn, P. Kim, J.-Y. Choi, B. H. Hong, *Nature* **2009**, *457*, 706–710.

[11] M. C. Duch, G. S. Budinger, Y. T. Liang, S. Soberanes, D. Urich, S. E. Chiarella, L. A. Campochiaro, A. Gonzalez, N. S. Chandel, M. C. Hersam, *Nano lett.* **2011**, *11*, 5201–5207.

[12] S. Pei, H.-M. Cheng, *Carbon* **2012**, *50*, 3210–3228.

[13] Y. Zhu, S. Murali, W. Cai, X. Li, J. W. Suk, J. R. Potts, R. S. Ruoff, *Adv. Mater.* **2010**, *22*, 3906–3924.

[14] X. Gao, J. Jang, S. Nagase, *J. Phys. Chem. C* **2009**, *114*, 832–842.

[15] W. Chen, L. Yan, P. R. Bangal, *Carbon* **2010**, *48*, 1146–1152.

[16] S. Stankovich, D. A. Dikin, R. D. Piner, K. A. Kohlhaas, A. Kleinhammes, Y. Jia, Y. Wu, S. T. Nguyen, R. S. Ruoff, *Carbon* **2007**, *45*, 1558–1565.

[17] Y. L. Zhang, L. Guo, H. Xia, Q. D. Chen, J. Feng, H. B. Sun, *Adv. Optical Mater.* **2014**, *2*, 10–28.

[18] G. Williams, B. Seger, P. V. Kamat, *ACS Nano* **2008**, *2*, 1487–1491.

[19] L. J. Cote, R. Cruz-Silva, J. Huang, *J. Am. Chem. Soc.* **2009**, *131*, 11027–11032.

[20] a) M. F. El-Kady, V. Strong, S. Dubin, R. B. Kaner, *Science* **2012**, *335*, 1326–1330; b) W. Gao, N. Singh, L. Song, Z. Liu, A. L. M. Reddy, L. Ci, R. Vajtai, Q. Zhang, B. Wei, P. M. Ajayan, *Nat. Nanotechnol.* **2011**, *6*, 496–500; c) H. Li, S. Pang, X. Feng, K. Müllen, C. Bubeck, *Chem. Commun.* **2010**, *46*, 6243–6245; d) Y. Matsumoto, M. Koinuma, S. Y. Kim, Y. Watanabe, T. Taniguchi, K. Hatakeyama, H. Tateishi, S. Ida, *ACS Appl. Mater. Interfaces* **2010**, *2*, 3461–3466.

[21] Y. Zhang, L. Guo, S. Wei, Y. He, H. Xia, Q. Chen, H.-B. Sun, F.-S. Xiao, *Nano Today* **2010**, *5*, 15–20.

[22] Y. Zhou, Q. Bao, B. Varghese, L. A. L. Tang, C. K. Tan, C. H. Sow, K. P. Loh, *Adv. Mater.* **2010**, *22*, 67–71.

[23] a) H. He, J. Klinowski, M. Forster, A. Lerf, *Chem. Phys. Lett.* **1998**, *287*, 53–56; b) A. Lerf, H. He, M. Forster, J. Klinowski, *J. Phys. Chem. B* **1998**, *102*, 4477–4482.

[24] a) D. Li, M. B. Mueller, S. Gilje, R. B. Kaner, G. G. Wallace, *Nat. Nanotechnol.* **2008**, *3*, 101–105; b) J. Paredes, S. Villar-Rodil, A. Martinez-Alonso, J. Tascon, *Langmuir* **2008**, *24*, 10560–10564.

[25] a) V. Eswaraiah, S. S. J. Aravind, S. Ramaprabhu, *J. Mater. Chem.* **2011**, *21*, 6800–6803; b) S. Gilje, S. Dubin, A. Badakhshan, J. Farrar, S. Danczyk, R. B. Kaner, *Adv. Mater.* **2010**, *22*, 419–423; c) X. H. Li, J. S. Chen, X. Wang, M. E. Schuster, R. Schlögl, M. Antonietti, *ChemSusChem* **2012**, *5*, 642–646; d) H. Zhang, Y. Miyamoto, *Phys. Rev. B* **2012**, *85*, 033402.

[26] V. A. Smirnov, A. Arbuzov, Y. M. Shul'ga, S. Baskakov, V. Martynenko, V. Muradyan, E. Kresova, *High Energy Chem.* **2011**, *45*, 57–61.

[27] a) S. Juodkazis, V. Mizeikis, K. K. Seet, M. Miwa, H. Misawa, *Nanotechnology* **2005**, *16*, 846; b) S. Kawata, H.-B. Sun, T. Tanaka, K. Takada, *Nature* **2001**, *412*, 697–698; c) C. N. LaFratta, J. T. Fourkas, T. Baldacchini, R. A. Farrer, *Angew. Chem. Int. Ed.* **2007**, *46*, 6238–6258; d) K.-S. Lee, R. H. Kim, D.-Y. Yang, S. H. Park, *Prog. Polym. Sci.* **2008**, *33*, 631–681; e) M. Malinauskas, M. Farsari, A. Piskarskas, S. Juodkazis, *Phys. Rep.* **2013**, *533*, 1–31; f) S. H. Park, D. Y. Yang, K. S. Lee, *Laser Photonics Rev.* **2009**, *3*, 1–11; g) Y.-L. Zhang, Q.-D. Chen, H. Xia, H.-B. Sun, *Nano Today* **2010**, *5*, 435–448.

[28] a) R. Mukherjee, A. V. Thomas, A. Krishnamurthy, N. Koratkar, *ACS Nano* **2012**, *6*, 7867–7878; b) V. Strong, S. Dubin, M. F. El-Kady, A. Lech, Y. Wang, B. H. Weiller, R. B. Kaner, *ACS Nano* **2012**, *6*, 1395–1403.

[29] F. Tuinstra, J. L. Koenig, *J. Chem. Phys.* **1970**, *53*, 1126–1130.

[30] L. Guo, R.-Q. Shao, Y.-L. Zhang, H.-B. Jiang, X.-B. Li, S.-Y. Xie, B.-B. Xu, Q.-D. Chen, J.-F. Song, H.-B. Sun, *J. Phys. Chem. C* **2012**, *116*, 3594–3599.

[31] L. Guo, Y. L. Zhang, D. D. Han, H. B. Jiang, D. Wang, X. B. Li, H. Xia, J. Feng, Q. D. Chen, H. B. Sun, *Adv. Optical Mater.* **2014**, *2*, 120–125.

[32] X. Wang, X. Li, L. Zhang, Y. Yoon, P. K. Weber, H. Wang, J. Guo, H. Dai, *Science* **2009**, *324*, 768–771.

[33] X. Li, H. Wang, J. T. Robinson, H. Sanchez, G. Diankov, H. Dai, *J. Am. Chem. Soc.* **2009**, *131*, 15939–15944.

[34] D. Wei, Y. Liu, Y. Wang, H. Zhang, L. Huang, G. Yu, *Nano Lett.* **2009**, *9*, 1752–1758.

[35] B. Guo, Q. Liu, E. Chen, H. Zhu, L. Fang, J. R. Gong, *Nano Lett.* **2010**, *10*, 4975–4980.

[36] N. Ashok Kumar, H. Nolan, N. McEvoy, E. Rezvani, R. L. Doyle, M. E. G. Lyons, G. S. Duesberg, *J. Mater. Chem. A* **2013**, *1*, 4431–4435.

[37] Y.-G. Bi, J. Feng, Y.-F. Li, Y.-L. Zhang, Y.-S. Liu, L. Chen, Y.-F. Liu, L. Guo, S. Wei, H.-B. Sun, *ACS Photonics* **2014**, *1*, 690–695.

[38] L. Guo, H.-B. Jiang, R.-Q. Shao, Y.-L. Zhang, S.-Y. Xie, J.-N. Wang, X.-B. Li, F. Jiang, Q.-D. Chen, T. Zhang, *Carbon* **2012**, *50*, 1667–1673.

[39] J. N. Wang, R. Q. Shao, Y. L. Zhang, L. Guo, H. B. Jiang, D. X. Lu, H. B. Sun, *Chem. Asian J.* **2012**, *7*, 301–304.

[40] a) J.-N. Wang, Y.-L. Zhang, Y. Liu, W. Zheng, L. P. Lee, H.-B. Sun, *Nanoscale* **2015**, *7*, 7101–7114; b) Y.-L. Zhang, Q.-D. Chen, Z. Jin, E. Kim, H.-B. Sun, *Nanoscale* **2012**, *4*, 4858–4869; c) Y.-L. Zhang, H. Xia, E. Kim, H.-B. Sun, *Soft Matter* **2012**, *8*, 11217–11231.

[41] H. B. Jiang, Y. L. Zhang, D. D. Han, H. Xia, J. Feng, Q. D. Chen, Z. R. Hong, H. B. Sun, *Adv. Funct. Mater.* **2014**, *24*, 4595–4602.

[42] Y.-L. Sun, W.-F. Dong, L.-G. Niu, T. Jiang, D.-X. Liu, L. Zhang, Y.-S. Wang, Q.-D. Chen, D.-P. Kim, H.-B. Sun, *Light Sci. Appl.* **2014**, *3*, e129.

[43] P. Theato, B. S. Sumerlin, R. K. O'Reilly, T. H. Epps III, *Chem. Soc. Rev.* **2013**, *42*, 7055–7056.

[44] a) D.-X. Lu, Y.-L. Zhang, D.-D. Han, H. Wang, H. Xia, Q.-D. Chen, H. Ding, H.-B. Sun, *J. Mater. Chem. C* **2015**, *3*, 1751–1756; b) Y. Tian, Y.-L. Zhang, H. Xia, L. Guo, J.-F. Ku, Y. He, R. Zhang, B.-Z. Xu, Q.-D. Chen, H.-B. Sun, *Phys. Chem. Chem. Phys.* **2011**, *13*, 4835–4838.

[45] T. Tatsuma, K. Takada, T. Miyazaki, *Adv. Mater.* **2007**, *19*, 1249–1251.

[46] H. Cheng, J. Liu, Y. Zhao, C. Hu, Z. Zhang, N. Chen, L. Jiang, L. Qu, *Angew. Chem. Int. Ed.* **2013**, *52*, 10482–10486.

[47] D. D. Han, Y. L. Zhang, H. B. Jiang, H. Xia, J. Feng, Q. D. Chen, H. L. Xu, H. B. Sun, *Adv. Mater.* **2015**, *27*, 332–338.

[48] D. D. Han, Y. L. Zhang, Y. Liu, Y. Q. Liu, H. B. Jiang, B. Han, X. Y. Fu, H. Ding, H. L. Xu, H. B. Sun, *Adv. Funct. Mater.* **2015**, *25*, 4548–4557.

[49] a) A. Castellanos-Gomez, L. Vicarelli, E. Prada, J. O. Island, K. Narasimha-Acharya, S. I. Blanter, D. J. Groenendijk, M. Buscema, G. A. Steele, J. Alvarez, *2D Mater.* **2014**, *1*, 025001; b) R. Mas-Balleste, C. Gomez-Navarro, J. Gomez-Herrero, F. Zamora, *Nanoscale* **2011**, *3*, 20–30; c) K. Novoselov, D. Jiang, F. Schedin, T. Booth, V. Khotkevich, S. Morozov, A. Geim, *Proc. Natl. Acad. Sci. USA* **2005**, *102*, 10451–10453.

[50] a) K. Ariga, Y. Yamauchi, G. Rydzek, Q. Ji, Y. Yonamine, K. C.-W Wu, J. P. Hill, *Chem. Lett.* **2014**, *43*, 36–68; b) D. Krishnan, F. Kim, J. Luo, R. Cruz-Silva, L. J. Cote, H. D. Jang, J. Huang, *Nano Today* **2012**, *7*, 137–152; c) Q. Ji, I. Honma, S.-M. Paek, M. Akada, J. P. Hill, A. Vinu, K. Ariga, *Angew. Chem. Int. Ed.* **2010**, *49*, 9737–9739; d) W. Strek, B. Cichy, L. Radosinski, P. Gluchowski, L. Marciniak, M. Lukaszewicz, D. Hreniak, *Light Sci. Appl.* **2015**, *4*, e237; e) Q. Li, N. Mahmood, J. Zhu, Y. Hou, S. Sun, *Nano Today* **2014**, *9*, 668–683; f) L. Wang, X. W. Lin, W. Hu, G. H. Shao, P. Chen, L. J. Liang, B. B. Jin, P. H. Wu, H. Qian, Y. N. Lu, X. Liang, Z. G. Zheng, Y. Q. Lu, *Light Sci. Appl.* **2015**, *4*, e253; g) W. Nakanishi, K. Minami, L. K. Shrestha, Q. Ji, J. P. Hill, K. Ariga, *Nano Today* **2014**, *9*, 378–394; h) D. Qu, M. Zheng, J. Li, Z. Xie, Z. Sun, *Light Sci. Appl.* **2015**, *4*, e364.